

# Tunable transmission of quantum Hall edge channels with full degeneracy lifting in split-gated graphene devices

Katrin Zimmermann,<sup>1,2</sup> Anna Jordan,<sup>1,2</sup> Frédéric Gay,<sup>1,2</sup> Kenji Watanabe,<sup>3</sup> Takashi Taniguchi,<sup>3</sup> Zheng Han,<sup>1,2</sup> Vincent Bouchiat,<sup>1,2</sup> Hermann Sellier,<sup>1,2</sup> and Benjamin Sacépé<sup>1,2,\*</sup>

<sup>1</sup>*Univ. Grenoble Alpes, Institut Néel, F-38000 Grenoble, France*

<sup>2</sup>*CNRS, Institut Néel, F-38000 Grenoble, France*

<sup>3</sup>*National Institute for Materials Science, 1-1 Namiki, Tsukuba 306-0044, Japan*

Charge carriers in the quantum Hall regime propagate via one-dimensional conducting channels that form along the edges of a two-dimensional electron gas. Controlling their transmission through a gate-tunable constriction, also called quantum point contact (QPC), is fundamental for many coherent transport experiments. However, in graphene, tailoring a QPC with electrostatic gates remains challenging due to the formation of p-n junctions below gate electrodes along which electron and hole edge channels co-propagate and mix, short-circuiting the constriction. Here we show that this electron-hole mixing is drastically reduced in high mobility boron-nitride/graphene/boron-nitride van-der-Waals heterostructures thanks to the full degeneracy lifting of the Landau levels, enabling QPC operation with full channel pinch-off. We demonstrate gate-tunable selective transmission of quantum Hall edge channels through the QPC, both in the integer and the fractional quantum Hall regimes. This gate-control of edge channel propagation in graphene van-der-Waals heterostructures opens the door to quantum Hall interferometry and electron quantum optics experiments in the integer and fractional quantum Hall regimes of graphene.

In two-dimensional electron gases formed in semiconductor heterostructures, confinement of electron transport through nano-patterned constrictions has led to tremendous advances in quantum transport experiments [1]. Chief among key devices, operating both at zero magnetic field and in the quantum Hall (QH) regime under strong magnetic field, is the quantum point contact: A gate-defined narrow and short constriction that enables control over the exact number of transmitted electronic modes between two reservoirs of electrons, leading to conductance quantization [2–7]. In the QH regime, fine tuning of transmission across the QPC via electrostatic gating has become essential for many experiments based on electron tunneling and charge partitioning, such as shot noise measurements [8, 9], quantum Hall interferometry [10, 11], and electron quantum optics [12, 13].

Yet, in monolayer graphene, demonstration of QPC operation in split-gate geometry remains challenging. The

major hurdle precluding engineering split-gated constrictions stems from the gapless graphene electronic band structure [14]. Depletion of an electron-doped region with a gate electrode indeed leads to a hole-doped region, creating a conducting, gapless p-n junction that inevitably short-circuits the constriction.

The alternative route that consists in confining electron transport through etched constrictions has long been difficult due to the fact that physically etched constrictions in low mobility devices are subject to electron localization by disorder and charging effects [15–18]. Recent improvements in device fabrication techniques have solved these issues with a significant rise of graphene mobility, mitigating disorder effects. In turn, remarkable etched constrictions in suspended graphene flakes were realized, showing clear conductance quantization upon varying the global device charge carrier density at zero magnetic field [19], and later confirmed in encapsulated graphene devices [20].

In the quantum Hall regime, tunability of the QPC constriction with split-gate electrodes is mandatory to control the transmission of QH edge channels and the tunneling between counter-propagating QH edge channels. However, the p-n junction formed along gate electrodes also poses problems as electron type QH edge channels co-propagate along the junction with hole type edge channels, as illustrated in Fig. 1a. First experiments in devices equipped with a single top-gate have shown that disorder promotes charge transfer between these co-propagating electron and hole edge channels, leading to chemical potential equilibration [21–23]. Recently, it has been shown that the use of boron-nitride (hBN) substrates that considerably reduces disorder can suppress equilibration effects at the pn interface in single top-gate devices [24]. The origin of this suppression remains unclear and could result from the opening of a gap at the charge neutrality point as observed in some graphene-on-hBN devices [25, 26]. For the split-gate defined QPC geometry, experiments in graphene QPC devices operating on the fourfold degenerate Landau levels (LLs) showed that the presence of QH edge channel mixing is indeed detrimental as it creates a short-circuit of the constriction via localized channels beneath the split-gates (red channels in Fig. 1a), thus hindering gate-control of QH edge channel transmission through the QPC [27, 28].

In this work we employ high mobility (hBN)/graphene/hBN van-der-Waals heterostructures [29, 30] to take advantage of the full symmetry breaking of the LLs and the emergence of an energy gap between electron and hole LLs, which significantly mitigate QH edge channel mixing. The heterostructures are equipped with back-gate and split-gate electrodes to realize QPC devices operating in the quantum Hall regime. By continuously changing the graphene electron densities in the bulk and beneath the split-gates, we identify the exact edge channel configurations for which QH edge channels are immune to short-circuiting. This enables to selectively gate-tune the transmission of both integer and fractional QH edge channels through the QPC, eventually leading to full pinch-off.

## RESULTS

### Split-gated high mobility graphene devices.

High mobility samples were fabricated following the recent tour de force in graphene device fabrication techniques using van-der-Waals pick-up [30], which produces remarkably clean encapsulation of graphene in between two hBN flakes (see Supplementary Information for details). In this configuration a top hBN layer serves naturally as a high quality dielectric for gating. Suitable etching of the hBN/graphene/hBN structure enables deposition of both contact electrodes on the edge of the heterostructure and split-gate electrodes in a single metal deposition step (see Fig. 1b).

In this study two different devices were fabricated, each showing quantitatively identical behaviors (see Supplementary Information). We present here the results of an hBN (17 nm)/graphene/hBN (32 nm) structure patterned in a  $2\ \mu\text{m}$  wide Hall bar with 6 contacts, and split-gates of  $150\ \text{nm}$  gap located in the central part of the device (see Fig. 1a). The  $\text{SiO}_2(285\text{nm})/\text{Si}^{++}$  substrate serves as a back-gate. The 6 contacts enable measurement of three voltages (see Fig. 1b) in 4-terminal configurations, leading to the longitudinal and diagonal resistances  $R_L$  and  $R_D$ , and the Hall resistance  $R_H$ . All measurements were carried out at a temperature of  $0.05\text{K}$ .

Figure 1c shows a map of  $R_L$  versus back-gate and split-gate voltages,  $V_{bg}$  and  $V_{sg}$  respectively, at zero magnetic field. The charge neutrality point (CNP) of the bulk graphene – the resistance peak independent of  $V_{sg}$  – is located at  $V_{bg}^{CNP} = -1\text{V}$  indicating very small residual doping. The diagonal line drawn by a second peak in  $R_L$  indicates charge neutrality in the split-gated region of graphene. Its slope corresponds to the ratio of capacitances between back-gated and split-gated regions ( $C_{sg}/C_{bg} = 7$ ) and hence provides a way to assess quantitatively for the charge carrier density beneath the split-gates (using  $C_{bg} = 11.1\text{nF}/\text{cm}^2$ ).

Analysis of transport properties at  $V_{sg} = 0\text{V}$  leads

to a mean free path of  $1.8\ \mu\text{m}$  that coincides with the width of the Hall bar, and a bulk mobility superior to  $200\,000\ \text{cm}^2\text{V}^{-1}\text{s}^{-1}$  at a charge carrier density of  $n \sim 10^{12}\ \text{cm}^{-2}$ . These, together with signatures of negative non-local resistance (Supplementary Fig. 1), demonstrate ballistic transport in the device.

The quality of our device is also apparent in the resolution of broken symmetry states of graphene in the QH regime at moderate magnetic field ( $B$ ). Figure 1d shows a color map of  $R_L$  versus  $V_{bg}$  and  $B$  taken at  $V_{sg} = 0\text{V}$ . In this Landau fan diagram,  $R_L = 0$  blue strips indexed by their respective integer value of the bulk filling factor  $\nu_b = n\phi_0/B$  ( $n$  is the carrier density and  $\phi_0 = h/e$  the flux quantum with  $e$  the electron charge and  $h$  the Planck constant) signal the presence of QH states. In addition to the usual graphene sequence  $\nu_b = 4(N + \frac{1}{2}) = 2, 6, 10, \dots$  where  $N$  is the LL index, symmetry breaking states at  $\nu_b = 1$  and at half-filling  $\nu_b = 4, 8, 12$ , are visible at fields as low as  $B = 3\text{T}$ . At  $B > 5\text{T}$ , LL degeneracies are fully lifted for  $N = 0, 1$  and  $2$  with clear additional minima at  $\nu_b = 1, 3, 5, 7$  and  $9$ . Importantly, the  $\nu = 0$  state that separates electron from hole states at  $V_{bg}^{CNP}$  shows insulating behavior with a diverging  $R_L$ , consistent with previous reports pointing to a gapped ground state [31–35]. At our highest  $B$  ( $14\text{T}$ ), these broken symmetry states are furthermore accompanied by fractional QH plateaux that are pronounced in the Hall conductance (Supplementary Fig. 2).

**QPC operation in the integer quantum Hall regime.** Let us now investigate the control of integer QH edge channels by split-gate electrodes defining the QPC. We begin with a set of data taken at  $B = 7\text{T}$  in the n-doped regime ( $V_{bg} > V_{bg}^{CNP}$ ). Figure 2a displays the color map of the diagonal conductance  $G_D = 1/R_D$  across the split-gates versus  $V_{bg}$  and  $V_{sg}$ . For negative  $V_{sg}$ , conductance plateaux quantified in units of  $e^2/h$  draw diagonal strips spanning a large range of  $V_{bg}$ , this voltage controlling the bulk filling factor  $\nu_b$  (labeled on the right axis). At positive  $V_{sg}$ , these diagonal strips break up into rhombi that are horizontally delimited by the width of the bulk QH plateaux, centred at integer values of  $\nu_b$ . Diagonal grey dotted lines index the expected filling factor beneath the split-gates,  $\nu_g$ , related to the local charge carrier density (extracted from Fig. 1c). These lines, together with  $\nu_b$  labels, give the exact QH edge channel configuration beneath the split-gates and in the bulk at any  $(V_{bg}; V_{sg})$ .

We first focus on the negative  $V_{sg}$  regime where the charge carrier density below the split-gates is lower than the graphene bulk density, as is required for confining bulk QH edge channels into the QPC. Inspecting the conductance strips we note that their slope does not match the lines of constant  $\nu_g$ . The shallower slope rather indicates a smaller capacitive coupling to the split-gate electrodes and hence a region of the graphene device with a charge carrier density in between those of the bulk

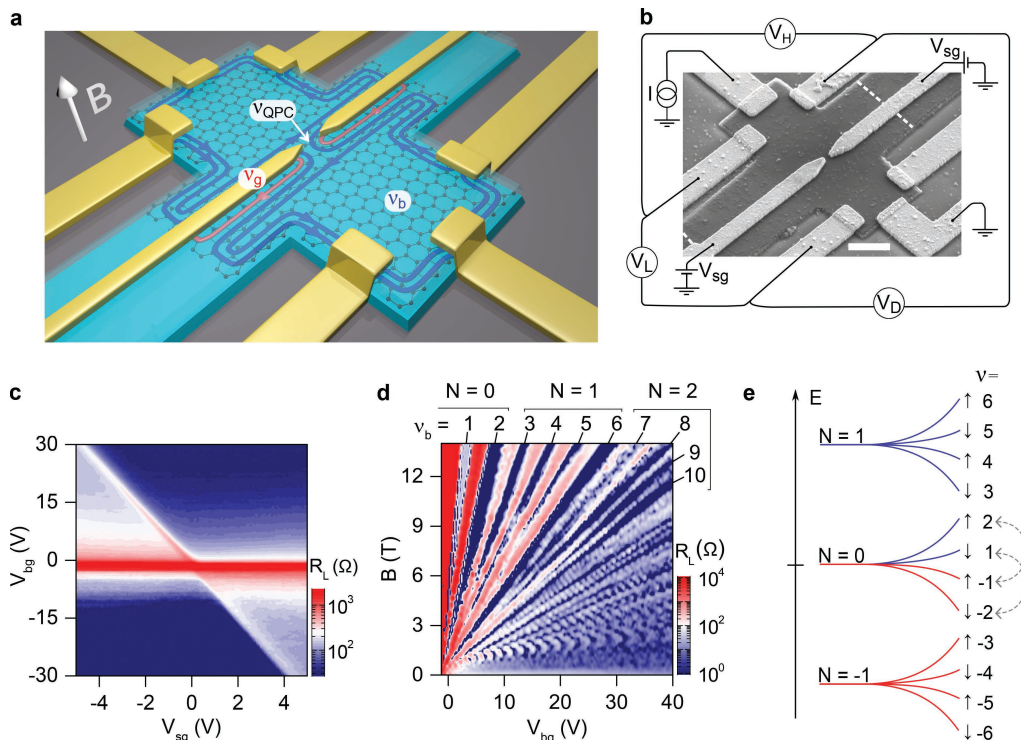


**FIG. 1. QPC device on hBN/graphene/hBN heterostructure.** (a) Schematic of the device showing graphene encapsulated in hBN (top hBN flake semi-transparent) with electrodes contacting the graphene on the edge of the heterostructure. Edge channels formed at high magnetic field are shown as red (hole) and blue (electron) channels.  $\nu_b$ ,  $\nu_g$  and  $\nu_{QPC}$  are the filling factors in the bulk, split-gates and QPC regions respectively and determine the number and type of edge channels present. For this schematic  $\nu_b = 2$ ,  $\nu_g = -1$  and  $\nu_{QPC} = 1$ . (b) Scanning electron micrograph of the device showing the measurement configurations. White dotted lines show the graphene edge buried below the hBN top layer. Scale bar is  $1\mu\text{m}$ . (c) Longitudinal resistance  $R_L$  as a function of back-gate and split-gate voltages at zero magnetic field. (d) Landau fan diagram of longitudinal resistance measured at 0.05K with floating split-gates. Indexed blue strips indicate bulk QH states. (e) Energy diagram showing degeneracy lifting of the  $N = -1, 0$  and  $1$  LLs into broken symmetry states indexed by the filling factor  $\nu$ . Arrows indicate the spin polarization of each electron (blue) and hole (red) level. Gray dashed arrows indicate the specific spin-selective equilibration restricted to the  $N = 0$  LL.

and the split-gates. This region is nothing but the QPC saddle-point constriction, which is capacitively coupled to both the back-gate and the split-gate electrodes. We thus introduce a third filling factor  $\nu_{QPC}$  related to the charge carrier density in the QPC (see Fig. 1a). In the following, we demonstrate that this framework provides a fully consistent understanding of our data.

For negative  $V_{sg}$ , the filling factor configuration is  $\nu_g < \nu_{QPC} < \nu_b$ , where inner bulk edge channels are expected to be successively back-reflected at the QPC (e.g. Fig. 1a). We first discuss the diagonal strips in yellow, red and dark red. Near zero split-gate voltage, charge carrier density is homogeneous in the whole graphene device, and  $\nu_g = \nu_{QPC} = \nu_b$  with  $\nu_b = 2, 3$ , and  $4$  respectively. At these points the conductance values of  $2e^2/h$ ,  $3e^2/h$ , and  $4e^2/h$  are those of the respective bulk QH plateaux defined by  $\nu_b$ . The key feature of this series of strips is that their conductance remains constant for any higher  $\nu_b$  and any lower  $\nu_g$ , indicating that only  $2, 3$  and  $4$  QH edge channels remain transmitted across the QPC,

even if the number of edge channels increases in the bulk or decreases below the split-gates. This clearly demonstrates that the strip conductance depends on the filling factor in the QPC and hence on the number of transmitted bulk edge channels. The diagonal conductance thus follows:

$$G_D = \frac{e^2}{h} \nu_{QPC}, \quad (1)$$

where  $\nu_{QPC}$  counts the number of transmitted edge channels, as expected for standard QPC devices [6]. Consequently we can index  $\nu_{QPC}$  according to (1) with the conductance value of each strip (the resulting values are labeled at the top of Fig. 2a).

This picture is further borne out by looking at the closing of the QPC with decreasing  $V_{sg}$  from zero at fixed  $V_{bg}$ . Figure 2c shows line-cuts of  $G_D$  versus  $\nu_{QPC}$  extracted from Fig. 2a at  $\nu_b = 3$  and  $4$ . The dark red curve taken at  $\nu_b = 4$  exhibits a plateau of  $G_D = 4e^2/h$  at  $\nu_{QPC} = 4$  when four bulk QH edge channels are transmitted. Reducing  $\nu_{QPC}$  to  $3$  by decreasing  $V_{sg}$  enables

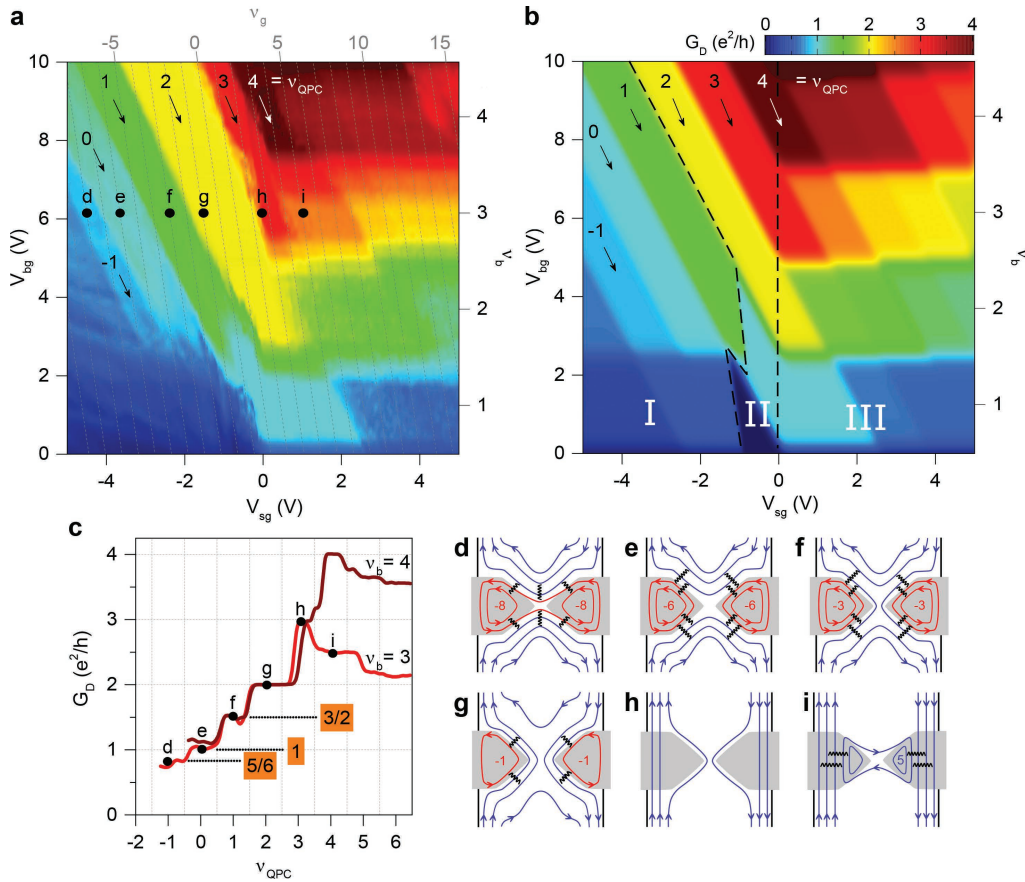


FIG. 2. **QPC in the quantum Hall regime.** (a) Diagonal conductance  $G_D$  as a function of back-gate and split-gate voltages,  $V_{bg}$  and  $V_{sg}$  respectively. The bulk filling factor  $\nu_b$  is labeled on the right axis. The gray dotted lines indicate constant filling factor below the split-gates and are indexed by  $\nu_g$  on the top-axis. The diagonal arrows indicate constant QPC filling factor  $\nu_{QPC}$ . Note that the sample is current biased precluding measurement of vanishing conductance at full pinch-off. (b) Computed diagonal conductance map divided into three regions that delimit different operating regimes. In region I the QPC is short-circuited by equilibration through the localized states beneath the split-gates. Region II defines the QPC operating regime. Region III is analogue to n-n'-n top-gated structures. (c)  $G_D$  versus  $\nu_{QPC}$  for  $\nu_b = 3$  and 4. The black dots labeled d-i correspond to the ones in (a). The labels 3/2, 1 and 5/6 highlight the anomalous conductance values due to equilibration in region I for  $\nu_{QPC} = 1, 0$  and  $-1$  respectively. (d-i) Edge channel configurations at the locations of the respective black dots in (a). Below the split-gates (gray areas), the numbers indicate  $\nu_g$ , with only the first two edge channels drawn. Equilibration between electron and hole channels is indicated by black wavy lines. (d)  $(\nu_b, \nu_g, \nu_{QPC}) = (3, -8, -1)$ , (e)  $(3, -6, 0)$ , (f)  $(3, -3, 1)$ , (g)  $(3, -1, 2)$ , (h)  $(3, 2, 3)$ , (i)  $(3, 5, 4)$ .

only 3 edge channels to pass through the QPC, leading to a plateau of  $G_D = 3e^2/h$ , and similarly for  $\nu_{QPC} = 2$  at lower  $V_{sg}$ . Therefore, closing the QPC by reducing the split-gate voltage leads to successive back-scattering of the inner edge channels demonstrating QPC operation in the integer QH regime.

Upon further closing the QPC, the situation becomes more complex. Decreasing  $V_{sg}$  to  $\nu_{QPC} = 1$  does not result in a conductance of  $e^2/h$ , but  $3/2e^2/h$  (green strip in Fig. 2a). Likewise, the conductance strips at  $\nu_{QPC} = 0$  and  $\nu_{QPC} = -1$  should show full pinch off with  $G_D \approx 0$ , but instead we observe conductance plateaux at  $\sim e^2/h$  and  $\sim 0.85e^2/h$  respectively for any  $\nu_b \geq 2$ .

The key to understanding these anomalous plateaux relies on a specific charge transfer –equilibration– be-

tween some of the back-reflected electron edge channels and some of the localized hole edge channels beneath the split-gates, thus adding a new conduction path short-circuiting the QPC. Following pioneering works on p-n junctions in graphene [21–23] and assuming full equilibration, we solved the current conservation law for the QPC geometry that now involves three filling factors  $\nu_b$ ,  $\nu_g$  and  $\nu_{QPC}$ , thus complexifying equilibration compared to n-p-n junctions (Supplementary Information). Taking into account that equilibration only occurs between QH edge channels of same spin polarization [24], the diagonal conductance reads:

$$G_D = \sum_{\sigma=\uparrow,\downarrow} G_D^{\nu_b^\sigma, \nu_g^\sigma, \nu_{QPC}^\sigma} \quad (2)$$

$$G_D^{\nu_b^\sigma, \nu_g^\sigma, \nu_{QPC}^\sigma} = \frac{e^2}{h} |\nu_b^\sigma| \frac{2|\nu_b^\sigma||\nu_g^\sigma| + \nu_{QPC}^\sigma(|\nu_b^\sigma| - |\nu_g^\sigma|)}{3|\nu_b^\sigma||\nu_g^\sigma| + |\nu_b^\sigma|^2 - 2\nu_{QPC}^\sigma|\nu_g^\sigma|} \quad (3)$$

where  $\nu_b^\sigma$ ,  $\nu_g^\sigma$  and  $\nu_{QPC}^\sigma$  count the number of sub-LLs of identical spin polarization  $\sigma$ . Here  $\nu_b^\sigma$  and  $\nu_g^\sigma$  are of opposite signs, whereas  $\nu_{QPC}^\sigma$  can be of both signs.

The fact that the conductance strips at  $\nu_{QPC} = 1$ , 0 and  $-1$  become anomalous from  $\nu_b = 2$  and stay constant for any higher  $\nu_b$  and any  $\nu_g < 0$  indicates that populating other LLs, namely  $N \geq 1$  in the bulk and  $N \leq -1$  under the split-gates, does not change the conductance. This finding thus points to equilibration uniquely between edge channels of the  $N=0$  LL. We therefore infer that charge transfer is restricted to occur between the spin upward  $\nu = 2$  and  $\nu = -1$  sub-LLs, and between the spin downward  $\nu = 1$  and  $\nu = -2$  sub-LLs, as indicated by the dotted arrows in the LL energy diagram in Fig. 1e.

As a result, for  $\nu_{QPC} = 1$  and  $\nu_b \geq 2$ , charge transfer between the back-reflected  $\nu_b = 2$  edge channel and the localized hole  $\nu_g = -1$  edge channel (see Fig. 2f) leads to  $G_D^{1^\uparrow, -1^\uparrow, 0^\uparrow} = 1/2 e^2/h$ . As the  $\nu_b = 1$  edge channel is transmitted through the QPC and contributes to  $e^2/h$  to the conductance, the sum of both contributions gives  $3/2 e^2/h$ , in agreement with the measured conductance value. For  $\nu_{QPC} = 0$  and  $\nu_b \geq 2$  as sketched in Fig. 2e, charge transfer between  $\nu_b = 1$  and  $\nu_g = -2$  edge channels (downward spin polarization), and between  $\nu_b = 2$  and  $\nu_g = -1$  edge channels (upward spin polarization) gives  $G_D^{1^\downarrow, -1^\downarrow, 0^\downarrow} = G_D^{1^\uparrow, -1^\uparrow, 0^\uparrow} = 1/2 e^2/h$ , thus a sum equal to  $e^2/h$ , as measured on the  $\nu_{QPC} = 0$  strip. For  $\nu_{QPC} = -1$ , a hole state connects the split-gates as sketched in Fig. 2d. In this case  $G_D^{1^\downarrow, -1^\downarrow, 0^\downarrow} = 1/2 e^2/h$  and  $G_D^{1^\uparrow, -1^\uparrow, -1^\uparrow} = 1/3 e^2/h$ , leading to a total conductance of  $5/6 e^2/h \simeq 0.83 e^2/h$ , remarkably close to our measurement. Consequently, spin-selective equilibration restricted to the  $N=0$  LL provides a full explanation of the anomalous conductance values of the strips when the filling factor in the QPC is reduced to 1, 0 or  $-1$ .

If we now consider positive  $V_{sg}$ , the filling factor configuration changes to  $\nu_b < \nu_{QPC} < \nu_g$ . Extra electron-type QH edge channels can thus connect left and right edges of the graphene device (see Fig. 2i) leading to chemical potential equilibration as in n-n'-n top-gated structures [23]. We observe spin-selective partial equilibration in this configuration, which is not restricted to the  $N = 0$  Landau level, resulting in fractional conductance values similar to those reported in high mobility graphene devices [24] (see Supplementary Information for further analysis).

The above analysis of the QPC diagonal conductance is computed in Fig. 2b, taking into account spin-selective equilibration for both  $V_{sg}$  polarities. Three distinct re-

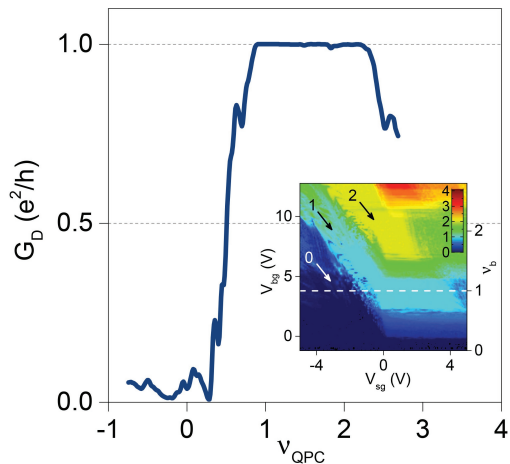


FIG. 3. **Full pinch-off.** Diagonal conductance  $G_D$  versus filling factor in the QPC  $\nu_{QPC}$  demonstrating a conductance drop to zero and thus full pinch-off. The curve is extracted at the white dashed line in the diagonal conductance map shown in the inset. (inset) Diagonal conductance versus back-gate and split-gate voltages measured at 14T and 0.05K in voltage bias configuration (excitation voltage of  $15\mu\text{V}$ ). The dark blue region corresponds to full pinch-off. The green strip at  $\nu_{QPC} = 1$  appears with some delay, suggesting less effective equilibration at higher magnetic field.

gions can be identified. In region I, equilibration restricted to the  $N = 0$  LL between reflected electron edge channels and localized hole states short-circuits the QPC leading to anomalous conductance plateaux. Region II defines the equilibration-free QPC device operating regime, where the conductance is precisely defined by the number of transmitted channels. Region III, at positive  $V_{sg}$ , describes the regime of n-n'-n unipolar equilibration. The remarkable one-to-one correspondence with our data of Fig. 2a supports the consistency of our analysis.

**Full pinch-off.** We complete this study of the QPC operation in the integer QH regime by addressing the pinch-off, which occurs for  $\nu_b = 1$  according to the dark blue triangle in region II in Fig. 2b. Figure 3 displays  $G_D$  versus  $\nu_{QPC}$  at  $\nu_b = 1$  extracted from a set of data taken at 14T (inset of Fig. 3). The conductance drops from  $e^2/h$  to a value  $< 0.1e^2/h$ , indicating full pinch-off of the  $\nu_b = 1$  QH edge channel, when  $\nu_{QPC} < 1$ . Interestingly, we observed in the conductance map shown in the inset of Fig. 3 that  $G_D$  remains vanishingly small (dark blue area) over a large range of gate values, indicating that equilibration is less efficient at 14T than at 7T, most likely due to the larger energy gaps.

**QPC operation in the fractional quantum Hall regime.** In the following, we turn to the QPC operation in the fractional QH regime. Owing to the high quality of our samples, fractional QH plateaux of the  $1/3$  family at  $\nu_b \pm 1/3$  develop at relatively low magnetic field of 14T [32, 33, 36, 37]. We observe plateaux in the bulk

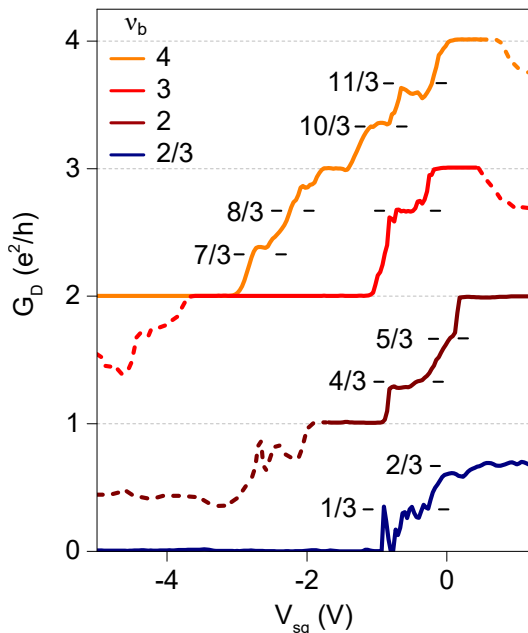


FIG. 4. **Pinch-off of fractional QH edge channels.** Diagonal conductance  $G_D$  versus  $V_{sg}$  for  $\nu_b = 4, 3, 2$  and  $2/3$  measured at 14T. Solid lines indicate the regime II of QPC operation, whereas dashed lines relates to the regime I and III. Reducing split-gate voltage unveils intermediate plateaux at fractional conductance values, which signal the successive back-reflection of fractional QH channels. The curves at  $\nu_b = 4, 3, 2$  are measured in current-bias configuration. The curve  $\nu_b = 2/3$  is measured in 4-terminal voltage-bias configuration, enabling measurement of the full pinch-off with  $G_D \approx 0$  at  $V_{sg} < -1V$ . The peaks in the transition to full pinch-off result from resonant tunneling between counter-propagating edge channels of the  $1/3$  fractional state [41].

Hall conductance accompanied with minima in longitudinal resistance at bulk filling factors  $1/3, 2/3, 4/3, 10/3$  and  $11/3$ . Other plateaux such as  $\nu_b = 7/3, 8/3$  have, however, lower fidelity with the expected quantized values (see Supplementary Fig. 2).

Akin to the integer QH effect, a key ingredient implicit in analysis of transport properties in the fractional QH regime is the existence of fractional QH edge channels [38, 39]. While their nature differs from the integer QH edge channels as they emerge from many-body interacting ground states within each LL [40], spatially separated edge channels are expected to propagate along the sample edges as evidenced by different means in GaAs [1]. In our graphene samples the QPC provides a perfect tool to unveil fractional edge channels by individually controlling their transmission.

Figure 4 displays  $G_D$  versus  $V_{sg}$  for  $\nu_b = 4, 3, 2$  and a fractional bulk value of  $2/3$ , all taken at 14T. Solid-lines indicate the region II of QPC operation. For  $\nu_b = 4$  at  $V_{sg} = 0$  conductance is that of the bulk:  $4e^2/h$ . Upon reducing  $V_{sg}$  the conductance decreases due to the back-reflection at the QPC of the inner  $\nu_b = 4$  edge channel,

and new intermediate fractional conductance plateaux emerge at  $(11/3)e^2/h$  and  $(10/3)e^2/h$ , before reaching the integer plateau of  $3e^2/h$ . Further pinching off reveals plateaux at  $(8/3)e^2/h$  and  $(7/3)e^2/h$ , though with less accurate conductance quantization. The  $8/3$  plateau is more pronounced for  $\nu_b = 3$ , whereas the  $7/3$  is absent. Similarly, on pinching off  $\nu_b = 2$ , a clear intermediate plateau at  $4/3$  emerges. Note that the small kink at  $G_D = (5/3)e^2/h$  signals the weak fractional state at  $\nu_b = 5/3$ , consistent with previous reports [36, 37]. Generalizing eq. (1) to the case of fractional filling factor  $\nu_{QPC}$  [38], all these intermediate plateaux therefore unveil the successive back-reflection at the QPC of the respective fractional QH edge channels and thus their very existence. Eventually, upon increasing pinch-off while starting at  $\nu_b = 2/3$ , a clear  $(1/3)e^2/h$  plateau emerges, followed ultimately, after its back-reflection, by a suppression of conductance indicating full QPC pinch-off.

## DISCUSSION

In two-dimensional electron gases buried in semiconductor heterostructures, the nature of the charge transfer between edge channels has been investigated at length [4, 5, 42, 43]. The overall picture is that any small amount of short-range disorder in real systems significantly enhances the tunneling rate between adjacent channels [44–46]. In case of two co-propagating channels at different chemical potentials, this inter-channel tunneling produces an out-of-equilibrium energy distribution that progressively relaxes to a new equilibrium by intra-channel inelastic processes. After complete equilibration, the current is equally distributed among channels that show identical chemical potential. In graphene, theoretical works showed that disorder and dephasing also drive equilibration at p-n junctions [47, 48]. However, consideration of selection rules on spin or valley indexes for equilibration between broken symmetry states is still lacking.

Interestingly, in our high mobility graphene devices, the regime of partial equilibration at  $V_{sg} > 0$  shows inter-Landau level equilibration, whereas in the QPC regime at  $V_{sg} < 0$ , equilibration is restricted to the  $N = 0$  Landau level. This difference can be accounted for by the distinct paths taken by the bulk QH edge channels in the two regimes. At  $V_{sg} > 0$ , bulk edge channels indeed keep propagating along the graphene edges below the split-gates, whereas for  $V_{sg} < 0$  they are guided along the p-n junctions. These two paths markedly differ by the shape of the local electrostatic potential, which is expected to be much smoother at the p-n junction than at the graphene edges. As the width of the incompressible strips that spatially separate edge channels are proportional to the ratio cyclotron gap over potential gradient [45], we expect the edge channels separation to be

significantly increased at the p-n junction, especially between the  $N = 0$  and  $N = 1$  Landau levels, which exhibit the largest cyclotron gap. As a result, at the p-n interface, the tunneling rate between edge channels of different Landau levels should be exponentially suppressed due to the large incompressible strips, precluding inter-Landau level mixing as observed in the QPC regime (Region I). Such conjectures that are based on electrostatics of QH edge channels call for further theoretical works including edge channel reconstruction and full degeneracy lifting of graphene QH states.

To conclude, our overall understanding of the precise edge channel configurations allows us to demonstrate gate-tunable and equilibration-free transmission of both integer and fractional QH edge channels through QPCs in graphene. Such a control of edge channel transmission enables future investigations of the equilibration processes at play that limit adiabatic transport [4, 5, 49], measurements of fractional charges [8, 9] in the multi-component fractional QH regime, design of single electron sources for electron quantum optics [12], quantum Hall interferometry [10, 11] or even more prospective devices based on coupling QH states with superconducting electrodes [50–52]. Our work thus opens the way to a wealth of invaluable experiments in graphene exploring the variety of new QH ground states of both the integer [34, 35] and fractional QH regimes [32, 33, 36, 37].

---

\* benjamin.sacepe@neel.cnrs.fr

- [1] C.W.J. Beenakker and H. van Houten, “Quantum transport in semiconductor nanostructures,” in *Semiconductor Heterostructures and Nanostructures*, Solid State Physics, Vol. 44, edited by Henry Ehrenreich and David Turnbull (Academic Press, 1991) pp. 1 – 228.
- [2] D. A. Wharam, T. J. Thornton, R. Newbury, M. Pepper, H. Ahmed, J. E. F. Frost, D. G. Hasko, D. C. Peacock, A. D. Ritchie, and G. A. C. Jones, “One-dimensional transport and the quantisation of the ballistic resistance,” *J. Phys. C* **21**, L209–L214 (1988).
- [3] B. J. van Wees, H. van Houten, C. W. J. Beenakker, J. G. Williamson, L. P. Kouwenhoven, D. van der Marel, and C. T. Foxon, “Quantized conductance of point contacts in a two-dimensional electron gas,” *Phys. Rev. Lett.* **60**, 848–850 (1988).
- [4] B. J. van Wees, E. M. M. Willems, C. J. P. M. Harmans, C. W. J. Beenakker, H. van Houten, J. G. Williamson, C. T. Foxon, and J. J. Harris, “Anomalous integer quantum hall effect in the ballistic regime with quantum point contacts,” *Phys. Rev. Lett.* **62**, 1181–1184 (1989).
- [5] L. P. Kouwenhoven, B. J. van Wees, N. C. van der Vaart, C. J. P. M. Harmans, C. E. Timmering, and C. T. Foxon, “Selective population and detection of edge channels in the fractional quantum hall regime,” *Phys. Rev. Lett.* **64**, 685–688 (1990).
- [6] M. Büttiker, “Absence of backscattering in the quantum hall effect in multiprobe conductors,” *Phys. Rev. B* **38**, 9375–9389 (1988).
- [7] M. Büttiker, “Quantized transmission of a saddle-point constriction,” *Phys. Rev. B* **41**, 7906–7909 (1990).
- [8] R. de Picciotto, M. Reznikov, H. Heiblum, V. Umansky, G. Bunin, and D. Mahalu, “Direct observation of a fractional charge,” *Nature* **389**, 162–164 (1997).
- [9] L. Saminadayar, D. C. Glattli, Y. Jin, and B. Etienne, “Observation of the  $e/3$  fractionally charged Laughlin quasiparticle,” *Phys. Rev. Lett.* **79**, 2526–2529 (1997).
- [10] B. J. van Wees, L. P. Kouwenhoven, C. J. P. M. Harmans, J. G. Williamson, C. E. Timmering, M. E. I. Broekaart, C. T. Foxon, and J. J. Harris, “Observation of zero-dimensional states in a one-dimensional electron interferometer,” *Phys. Rev. Lett.* **62**, 2523–2526 (1989).
- [11] Y. Ji, Y. Chung, D. Sprinzak, M. Heiblum, D. Mahalu, and H. Shtrikman, “An electronic mach-zehnder interferometer,” *Nature* **422**, 415–418 (2003).
- [12] G. Fève, A. Mahé, J.-M. Berroir, T. Kontos, B. Plaçais, D. C. Glattli, A. Cavanna, B. Etienne, and Y. Jin, “An on-demand coherent single-electron source,” *Science* **316**, 1169–1172 (2007).
- [13] B. Bocquillon, V. Freulon, J.-M. Berroir, P. Degiovanni, B. Plaçais, A. Cavanna, Y. Jin, and G. Fève, “Coherence and indistinguishability of single electrons emitted by independent sources,” *Science* **339**, 1054–1057 (2013).
- [14] A. H. Castro Neto, F. Guinea, N. M. R. Peres, K. S. Novoselov, and A. K. Geim, “The electronic properties of graphene,” *Rev. Mod. Phys.* **81**, 109–162 (2009).
- [15] M. Y. Han, B. Özyilmaz, Y. Zhang, and P. Kim, “Energy band-gap engineering of graphene nanoribbons,” *Phys. Rev. Lett.* **98**, 206805 (2007).
- [16] C. Stampfer, J. Güttinger, S. Hellmüller, F. Molitor, K. Ensslin, and T. Ihn, “Energy gaps in etched graphene nanoribbons,” *Phys. Rev. Lett.* **102**, 056403 (2009).
- [17] F. Molitor, A. Jacobsen, C. Stampfer, J. Güttinger, T. Ihn, and K. Ensslin, “Transport gap in side-gated graphene constrictions,” *Phys. Rev. B* **79**, 075426 (2009).
- [18] K. Todd, H.-T. Chou, S. Amasha, and D. Goldhaber-Gordon, “Quantum dot behavior in graphene nanoconstrictions,” *Nano Letters* **9**, 416–421 (2009).
- [19] N. Tombros, A. Veligura, J. Junesch, M.H.D. Guimaraes, I.J. Vera-Marun, H.T. Jonkman, and B.J. van Wees, “Quantized conductance of a suspended graphene nanoconstriction,” *Nat. Phys.* **7**, 697–700 (2011).
- [20] B. Terrés, L. A. Chizhova, F. Libisch, J. Peiro, D. Jörger, S. Engels, A. Girschik, K. Watanabe, T. Taniguchi, S. V. Rotkin, Burgdörfer J., and Stampfer C., “Size quantization of dirac fermions in graphene constrictions,” *Nat. Commun.* **7**, 11528 (2016).
- [21] J. R. Williams, L. DiCarlo, and C. M. Marcus, “Quantum hall effect in a gate-controlled p-n junction of graphene,” *Science* **317**, 638–641 (2007).
- [22] D. A. Abanin and L. S. Levitov, “Quantized transport in graphene p-n junctions in a magnetic field,” *Science* **317**, 641–643 (2007).
- [23] B. Özyilmaz, P. Jarillo-Herrero, D. Efetov, D. A. Abanin, L. S. Levitov, and P. Kim, “Electronic transport and quantum hall effect in bipolar graphene  $p$ - $n$ - $p$  junctions,” *Phys. Rev. Lett.* **99**, 166804 (2007).
- [24] F. Amet, J. R. Williams, K. Watanabe, T. Taniguchi, and D. Goldhaber-Gordon, “Selective equilibration of spin-polarized quantum hall edge states in graphene,” *Phys. Rev. Lett.* **112**, 196601 (2014).
- [25] B. Hunt, J. D. Sanchez-Yamagishi, A. F. Young, M. Yankowitz, B. J. LeRoy, K. Watanabe, T. Taniguchi,

- P. Moon, M. Koshino, P. Jarillo-Herrero, and R. C. Ashoori, “Massive Dirac Fermions and Hofstadter Butterfly in a van der Waals Heterostructure,” *Science* **340**, 1427–1430 (2013).
- [26] C. R. Woods, L. Britnell, A. Eckmann, R. S. Ma, J. C. Lu, H. M. Guo, X. Lin, G. L. Yu, Y. Cao, R. V. Gorbachev, A. V. Kretinin, J. Park, L. A. Ponomarenko, M. I. Katsnelson, Yu. N. Gornostyrev, K. Watanabe, T. Taniguchi, C. Casiraghi, H.-J. Gao, A. K. Geim, and K. S. Novoselov, “Commensurate-incommensurate transition in graphene on hexagonal boron nitride,” *Nat. Phys.* **10**, 451–456 (2014).
- [27] S. Nakaharai, J. R. Williams, and C. M. Marcus, “Gate-defined graphene quantum point contact in the quantum hall regime,” *Phys. Rev. Lett.* **107**, 036602 (2011).
- [28] S. Xiang, A. Mreńca-Kolasińska, V. Miseikis, S. Guiducci, K. Kolasiński, C. Coletti, B. Szafran, F. Beltram, S. Roddaro, and S. Heun, “Interedge backscattering in buried split-gate-defined graphene quantum point contacts,” *Phys. Rev. B* **94**, 155446 (2016).
- [29] A. K. Geim and I. V. Grigorieva, “Van der waals heterostructures,” *Nature* **499**, 419–425 (2013).
- [30] L. Wang, I. Meric, P. Y. Huang, Q. Gao, Y. Gao, H. Tran, T. Taniguchi, K. Watanabe, L. M. Campos, D. A. Muller, J. Guo, P. Kim, J. Hone, K. L. Shepard, and C. R. Dean, “One-dimensional electrical contact to a two-dimensional material,” *Science* **342**, 614–617 (2013).
- [31] J. G. Checkelsky, L. Li, and N. P. Ong, “Zero-energy state in graphene in a high magnetic field,” *Phys. Rev. Lett.* **100**, 206801 (2008).
- [32] X. Du, I. Skachko, F. Duerr, A. Luican, and A. Y. Andrei, “Fractional quantum hall effect and insulating phase of dirac electrons in graphene,” *Nature* **462**, 192–195 (2009).
- [33] K. I. Bolotin, F. Ghahari, M. D. Shulman, H. L. Stormer, and P. Kim, “Observation of the fractional quantum hall effect in graphene,” *Nature* **462**, 196–199 (2009).
- [34] A. F Young, C. R Dean, L. Wang, H. Ren, P. Cadden-Zimansky, K. Watanabe, T. Taniguchi, J. Hone, K. L. Shepard, and P. Kim, “Spin and valley quantum hall ferromagnetism in graphene,” *Nature Physics* **8**, 550–556 (2012).
- [35] A. F Young, J. D. Sanchez-Yamagishi, B. Hunt, S. H. Choi, K. Watanabe, T. Taniguchi, R. C. Ashoori, and P. Jarillo-Herrero, “Tunable symmetry breaking and helical edge transport in a graphene quantum spin hall state,” *Nature* **505**, 528–532 (2014).
- [36] C. R. Dean, A. F. Young, L. Cadden-Zimansky, P. Wang, K. Ren, H. and Watanabe, T. Taniguchi, P. Kim, J. Hone, and K. L. Shepard, “Multicomponent fractional quantum hall effect in graphene,” *Nature Physics* **7**, 693–696 (2011).
- [37] F. Amet, A. J. Bestwick, J. R. Williams, L. Balicas, K. Watanabe, T. Taniguchi, and D. Goldhaber-Gordon, “Composite fermions and broken symmetries in graphene,” *Nat. Commun.* **6**, 5838 (2014).
- [38] C. W. J. Beenakker, “Edge channels for the fractional quantum hall effect,” *Phys. Rev. Lett.* **64**, 216–219 (1990).
- [39] A. H. MacDonald, “Edge states in the fractional-quantum-hall-effect regime,” *Phys. Rev. Lett.* **64**, 220–223 (1990).
- [40] X. G. Wen, “Chiraluttinger liquid and the edge excitations in the fractional quantum hall states,” *Phys. Rev. B* **41**, 12838–12844 (1990).
- [41] F.P. Milliken, C.P. Umbach, and R.A. Webb, “Indications of a luttinger liquid in the fractional quantum hall regime,” *Solid State Commun.* **97**, 309–313 (1996).
- [42] B. W. Alphenaar, P. L. McEuen, R. G. Wheeler, and R. N. Sacks, “Selective equilibration among the current-carrying states in the quantum hall regime,” *Phys. Rev. Lett.* **64**, 677–680 (1990).
- [43] N. Paradiso, S. Heun, S. Roddaro, D. Venturelli, F. Taddei, V. Giovannetti, R. Fazio, G. Biasiol, L. Sorba, and F. Beltram, “Spatially resolved analysis of edge-channel equilibration in quantum hall circuits,” *Phys. Rev. B* **83**, 155305 (2011).
- [44] Th. Martin and S. Feng, “Suppression of scattering in electron transport in mesoscopic quantum hall systems,” *Phys. Rev. Lett.* **64**, 1971–1974 (1990).
- [45] D. B. Chklovskii, B. I. Shklovskii, and L. I. Glazman, “Electrostatics of edge channels,” *Phys. Rev. B* **46**, 4026–4034 (1992).
- [46] C. L. Kane and Matthew P. A. Fisher, “Contacts and edge-state equilibration in the fractional quantum hall effect,” *Phys. Rev. B* **52**, 17393–17405 (1995).
- [47] J. Li and S.-Q. Shen, “Disorder effects in the quantum hall effect of graphene  $p$ - $n$  junctions,” *Phys. Rev. B* **78**, 205308 (2008).
- [48] J.-C. Chen, H. Zhang, S.-Q. Shen, and Q.-F. Sun, “Dephasing effect on transport of a graphene pn junction in a quantum hall regime,” *Journal of Physics: Condensed Matter* **23**, 495301 (2011).
- [49] C. Altimiras, H. le Sueur, U. Gennser, A. Cavanna, D. Mailly, and F. Pierre, “Non-equilibrium edge-channel spectroscopy in the integer quantum hall regime,” *Nat. Phys.* **6**, 34 (2010).
- [50] L. Fu, “Electron teleportation via majorana bound states in a mesoscopic superconductor,” *Phys. Rev. Lett.* **104**, 056402 (2010).
- [51] P. San-Jose, J. L. Lado, R. Aguado, F. Guinea, and J. Fernández-Rossier, “Majorana zero modes in graphene,” *Phys. Rev. X* **5**, 041042 (2015).
- [52] F. Amet, C. T. Ke, I. V. Borzenets, J. Wang, K. Watanabe, T. Taniguchi, R. S. Deacon, M. Yamamoto, S. Bomze, Y. Tarucha, and G. Finkelstein, “Supercurrent in the quantum hall regime,” *Science* **352**, 966–969 (2016).

**Acknowledgments** We are grateful to D. Abanin, H. Baranger, Th. Champel, H. Courtois, C. Dean, S. Florens, M. Goerbig, L. Levitov, Y. Meir and D. Shahar for invaluable discussions. This work was supported by the Nanosciences Foundation of Grenoble and the H2020 ERC grant *QUEST* # 637815.